A tailored ceramic composite separator with electron-rich groups for high-performance lithium metal anode

A tailored ceramic composite separator with electron-rich groups for high-performance lithium metal anode

Lei Sheng [a,b], Xin Xie [a], Catia Arbizzani [b,**], Luca Bargnesi [b], Yaozong Bai [c], Gaojun Liu [c], Haoyu Dong [c], Tao Wang [a], Jianping He [a,*]

[a] College of Material Science and Technology, Nanjing University of Aeronautics and Astronautics, Nanjing, Jiangsu Province, 210016, China
[b] Department of Chemistry "Giacomo Ciamician", University of Bologna, Bologna, 40126, Italy
[c] Sinoma Lithium Battery Separator Co. Ltd, ZaoZhuang, Shandong province, 277500, China

Keywords:
Composite separator
Electron-rich groups
Interface capacitance
DFT
Lithium anode

A B S T R A C T

Ceramic composite separator is more competitive than traditional polyolefin separator in the field of power supply for superior thermal stability and wettability of liquid electrolyte. In this study, we develop a two-steps method that modifies SiO_2 with acrylamide (AM) by grafting process and prepare a functional SiO_2 composite separator (PE/SiO_2-AM). This kind of composite separator exhibits similar size-shrinkage (8.8%) to that of PE/ SiO_2 composite separator at the tested temperature, lower than 18.1% of bare PE separator, and is electro- chemically stable below 4.5 V (vs. Li/Li^+). In addition, the Li-symmetric cells employing PE/SiO_2-AM composite separator have the lowest overpotential and an improved lithium-ion transference number of 0.44. It is demonstrated from DFT calculation that the electron-rich species of imide group is able to uniformly disperse lithium-ion flux at the interface of electrolyte/lithium anode, and contributes to lithium-ion transport process. After assembling the $LiCoO_2$/Li half cells, the cell with PE/SiO_2-AM composite separator displays better cycle performance and higher discharge capacity when compared with other separators. Therefore, functional ceramic separator would be more attractive for next-generation lithium metal battery with high energy density.

1. Introduction

Separator is a crucial safety part inside lithium-ion batteries (LIBs), which can prevent cathode from directly contacting anode and mean- time allow lithium-ion pass. And it must possess excellent electronic insulation and ion conduction properties [1]. In the initial stage of LIBs, polyolefin (polypropylene (PP) or polyethylene (PE)) micropore mem- branes were favorite separators for their low-cost, great electrochemical stability and strong mechanical strength [2,3]. When liquid electrolyte is stored in porous polyolefin separator, lithium-ion can achieve the effective transportation between the cathode and the anode. With the boost of LIBs in energy storage facility and electric vehicle areas, all parts of LIBs need be optimized further or replaced to improve specific energy density [4,5].

In a traditional LIB, the specific capacity closely relates to the electrode materials, while soft polyolefin separator is only used with the role of physically separating the porous electrodes. Particularly, there is a little physical contact between flat separator and these powder electrodes. It is well-recognized that solid electrolyte interphase (SEI) at the negative electrode or cathode electrolyte interphase (CEI) at the positive electrode are formed during the first charge and discharge processes of cells, which would fill the space between separator and electrodes. Hence, a large part of researches about separators is focused on their thermal stability and the safety of LIBs. LIBs working at high tempera- ture [6,7] or high current [8] are challenging for conventional polyolefin-based separator, which could lead to serious incidents like thermal runaway. Novel nanofiber membranes or coating modification for polyolefin separator [9–11] has been widely reported recently. Generally, nanofiber membranes show highly porous structure and excellent electrolyte wettability, but its mechanical strengthen is still far inferior than commercial PP or PE separators. Therefore, in actual in- dustrial production, coating modification about polyolefin separator are attractive for stronger tension and well-operated. For example, Martinez-Cisneros et al. have demonstrated that tri-layers separators

* Corresponding author.
** Corresponding author.
E-mail addresses: catia.arbizzani@unibo.it (C. Arbizzani), jianph@nuaa.edu.cn (J. He).

(PP/PE/PP) appear to be the most efficient alternative to prevent thermal runaway, since PE provides a lower shutdown temperature, while PP still achieves mechanical stability at and above melting temperature of PE [12]. This pre-warning mechanism is ingeniously based on differences in the thermal stability of different polymers. Similarly, Ai et al. have also tried to coat a commercial PP separator with a thin layer of low-density polyethylene microspheres (PM). The composite separator cuts off the ion transportation between the electrodes and interrupts the battery reaction for blocking off the pores of the PP substrate within very short time periods: 3 s at 110 ˚C and 1 s at 120 ˚C [13].

On the other hand, a general "armour" strategy, with the inorganic ceramic particles (Al_2O_3 [14,15], SiO_2 [16–18], TiO_2 [19–21], ZrO_2 [22], CeO_2 [23], etc.) coated onto the surface of polymer-based sepa- rators, is beneficial to maintain dimensional stability of polymer matrix under extreme environment. For instance, in 2010, Kim et. Al have prepared a kind of tri-layers separator with inorganic particulate film/poly(methyl methacrylate) (PMMA)/inorganic particulate film via a simple dip-coating process. This tri-layers separator undergoes the lowest degree of dimensional change after storing at 150 ˚C for 20 min when compared with the PE separator, pure PMMA film [12]. This has aroused people's strong attention to the ceramic composite separators. A lot of works about optimizing the ceramic layer such as coating method [24–27], ceramic particle size [28], morphology [29,30] or surface modification [31–34], and binder [35–37] have been carried out in recent years. For instance, Jung et al. have tried to coat 10 nm Al_2O_3-- layer onto the surface of PP separator via atomic layer deposition (ALD) technology, with a rarely increased total separator thickness [38]. Besides, in order to design an eco-friendly preparation route of ceramic composite separator, some water-soluble binders such as CMC and polyacrylic acid (PAA) have been also reported in the literature [31,36, 37].

With the deepening of research on separators, a trend gradually occurs from safety parts to functional components. Some customized coats have been tailored to address the problems that shuttle of soluble species in the cathode region or precipitated lithium in the anode region, especially in the renaissance of lithium metal batteries (LMBs) [39–42]. For instance, Halalay et al. have promoted an effective method that Mn cation can be trapped by polymeric aza-15-crown-5 ethers. They have revealed that the content of Mn on the coated separator is far more than that of Mn deposited at the negative electrode [43]. Furthermore, it is also worth noting that the separator has an influence on the transport of lithium-ion and on the distribution of lithium-ion near the lithium anode [44,45]. More and more functional coats for separator have been reported in recent years, such as metal organic framework (MOF, NH_2-MIL-125) [46], covalent organic framework (COF, TPB-DMTP) [47] and zeolites [48] etc. It is believed that these porous materials with well-defined intrinsic nanochannels or negatively charged gap channels are able to facilitate lithium-ion transport. Also, fast ion conductors like $Li_{6.75}La_3Zr_{1.75}Ta_{0.25}O_{12}$ (LLZTO) [49,50], $Li_{1.3}Al_{0.3}Ge_{1.7}(PO_4)_3$ (LAGP) [51] and $PbZr_{0.52}Ti_{0.48}O_3$ (PZT) [52] are used to fabricate composite separators, and effectively redistribute uneven Li^+ flux coming from the insulated polyolefin separator. Additionally, some ceramic particles like Al_2O_3, SiO_2, and TiO_2, modified by $–NH_2$ [53], $–CONH_2$ [54] and –F [55,56] groups, have stronger negative charge effect for lone pair electrons or electronegativity, which would stabilize or promote the transport of lithium ion. To improve thermal stability and ion-transporting properties of separator, in this study, we have prepared SiO_2 particles with amide group (SiO_2-AM) by surface modification, and have coated them onto the surface of PE separator. During the half-cells test, the SiO_2-AM layer is faced with lithium metal anode, which is hope to stabilize lithium-ions at the interface of electrode/electrolyte and uniform the flux of lithium-ion.

2. Experimental

2.1. Materials

Tetraethyl orthosilicate (TEOS, AR), acrylamide (AM, AR), ethanol (CH_3CH_2OH), dimethyl formamide (DMF, AR) and ammonium hydroxide ($NH_3\ H_2O$, 28%wt, AR) were purchased from Sinopharm Chemical Reagent Co. Ltd (China). Vinyl trimethoxy silane (VTMS, AR) were bought from Aladdin Chemical Reagent Co. Ltd (China). The PE separator (the thickness is $1.6*10^{-3}$ cm) was kindly supported by Sinoma Lithium Battery Separator Co. Ltd (China). The $LiCoO_2$ electrode and polyvinylidene difluoride (PVDF) binder were supplied from Shenzhen Kejin Co. Ltd (China). Organic liquid electrolyte, 1 M $LiPF_6$ in dimethyl carbonate/ethylene carbonate (DEC/EC, 1:1 by volume) with 5% fluoroethylene carbonate (FEC), were bought from DoDoChem Co. Ltd (China) and stored in the glovebox.

2.2. Synthesis of SiO_2-AM particles

SiO_2 particles were synthesized via a Stober method. 16 mL of $NH_3\ H_2O$ and 10 mL of H_2O were firstly put into a flask with 164 mL of ethanol, and the mixture been stirred at room temperature for 0.5 h. After that, 10 mL of TEOS was added into this homogeneous solution at 40 ˚C and stirred for 4 h. Finally, the opacified solution were centrifuged to obtain SiO_2 particles. And these SiO_2 particles were washed by ethanol for three times and then dried in a vacuum oven at 60 ˚C for 24 h.

A certain amount of SiO_2 particles power, 10 ml of ammonium hydroxide, 5 mL of VTMS and 10 ml of H_2O were firstly added into 150 mL of ethanol solution and dispersed by continuous magnetic stirring at 40 ˚C for 12 h. Then, 4 g AM, 0.4 g $K_2S_2O_8$, and 10 ml H_2O were put into homogeneous mixture for 4 h at 70 ˚C. Finally, the centrifuged SiO_2-AM particles were washed using deionized water and acetone for three times, respectively, and then dried in a vacuum oven at 60 ˚C for 24 h.

2.3. Preparation of SiO_2-AM/PE composite separators

We firstly prepared the coating slurry by PVDF as the binder and DMF as the solvent. 0.1 g of PVDF powder and 0.9 g of SiO_2-AM particles were added into in a glass bottle with DMF liquid. After that, this mixture was continuously stirred for 24 h at room temperature. The homogeneous slurry was obtained and finally coated onto one side of PE separator via a scraping knife. And the SiO_2-AM/PE composite separator was dried in a vacuum oven at 80 ˚C for 12 h. For comparison, the SiO_2/ PE composite separator was also prepared using pure SiO_2 nanoparticles via the same method. The thickness of these composite separators was controlled about $2.2*10^{-3}$ cm.

2.4. Characterization and measurements

All separators are firstly sprayed with gold and then the morphology is observed at an operating voltage of 5 kV by the scanning electron microscope (SEM, S-4800, Hitachi, Japan). The sample was quenched to break with liquid nitrogen and then observe the cross-sectional SEM images. In the high-magnification SEM image, the diameter distribution of 50 sample particles is randomly counted via the ImageJ software analysis and the image scale. And FTIR-ATR (Bruker Optics, Switzerland) was served to analyze the chemical compositions of separators at a range of 400–4000 cm^{-1}. X-ray photoelectron spectroscopy (XPS) was measured ranging from 0 eV to 1100 eV (Thermo ESCALAB 250XI, America). An UV–Vis–NIR spectrophotometer (UV-2550, Shimadzu, Japan) was used to test the absorption characteristic of these samples in the wavelength range of 200–2500 nm, and $BaSO_4$ was used as a reference. A thermogravimetric analyzer (TGA-Q50, TA instruments, America) test is used to evaluate the thermal stability of ceramic particles and processed at the temperature range of 25–550 ˚C

with a heating rate of 25 °C min^{-1} in Ar atmosphere. The measurement of crystal structure and orientation was carried out using a wide-angle X- ray diffractometer (WAXD, Bruker, Germany) with Cu Kα X-ray radia- tion (λ = 0.154 nm). The contact angle test was performed with a device (SL200B, Solon Tech., China) and it was used to evaluate the surface property of all separators. Distilled water and organic liquid electrolyte were regarded as the using liquids of contact angle, respectively. The separator is weighted before and after immersed in the organic elec- trolyte, respectively. And the electrolyte uptake of these separators was measured by this equation (1) of $w(\%) = (W_{wet} - W_{dry})/ W_{dry}$, where W_{wet} represents the weight of separators after soaking organic electrolyte (1.0 M $LiPF_6$/EC + DEC (wt/wt = 1:1) with 5% FEC), W_{dry} is the weight of dry separator. The test of thermal stability was proceeded at 135 °C or 150 °C for 30 min in a thermocirculator oven, and the size shrinkage of separators was measured before and after heat-treatment. Due to the battery operating at the high voltage, the electrochemical stability of inter separators need to be evaluated by linear sweep voltammetry (LSV) [57]. We put the separator between the stainless steel and lithium metal, which are regarded as working electrode and counter electrode, respectively. The latter acted also as reference electrode. The detail testing program is carried out from 3 V to 6 V at a rate of 5 mV s^{-1} by the electrochemical workstation (Solartron 1287, USA). Besides, in order to evaluate the transport performance of lithium ions inside the separator, the transference number of lithium-ion is measured by a Li-symmetric cell, which is composed of two lithium metal electrodes. The cells containing different separators were tested with the potentiometric polarization (Solartron 1287, USA) and electrochemical impedance spectroscopy (Solartron 1260, USA) techniques. The polarization process is lasting for 1200 s with a small DC potential (5.0 mV) to achieve a steady-state current. The impedance spectra were recorded before and after polarization in range of 10^{-1} Hz–10^5 Hz with an AC voltage of 10 mV and 10 points/decade. Finally, t_{Li}^+ could be calculated with equation (2) of $t_{Li^+} = I_s(\Delta V - I_0R_0)/I_0(\Delta V - I_sR_s)$, where ΔV is the small DC polarization potential (5.0 mV), I_s and I_0 represent the steady-state current and initial current, respectively. R_s and R_0 represent the interfacial impedance after and before polarization, respectively. Furthermore, the Li-symmetric cells were also used to explore the morphology of separator after long-cycles. When the areal capacity is Q (mAh), the actual area is S (cm^2), the theoretical thickness of Li deposited layer *L* is calculated using equation (3):

$$L\ (\mathrm{cm}) = \frac{3.6\ Q^*\ M_{Li}}{e^{-}{}^*\ N_A{}^*\ \rho_{Li}{}^*S} = \frac{4.85{}^*Q}{10^4{}^*S}$$

where the elementary charge (e^-) is 1.602 * 10^{-19}, the Avogadro number (N_A) is 1.602 * 10^{23}, the molar mass (M_{Li}) is 6.94 g mol^{-1}, the density (ρ_{Li}) is 0.534 g cm^{-3}.

To evaluate the battery performance, the CR-2032 type coin cells containing a commercial $LiCoO_2$ cathode (11.7 mg cm^{-2}, the diameter is 1.2 cm), lithium metal anode (the diameter is 1.6 cm, the thickness is 0.5 cm) and liquid electrolyte (90 μL), were assembled with different separators, respectively. The Li-symmetric cells were composed of the same lithium electrodes and liquid electrolyte (60 μL). All assembling process of cells were conducted in a glovebox with argon atmosphere (the content of O_2 < 0.1 ppm and H_2O < 0.1 ppm). The charging and discharging process of these cells was performed on a battery testing equipment (CT2001A, Land, China). For the evaluation of the cell cycling and rate capability performance, the voltage ranges from 3 V to 4.4 V. While cycling stability was evaluated at 1 C, the rate capability tests were performed at a charge rate of 0.2C, and discharge rate of 0.2C, 0.5C, 1 C, 2 C and 3 C, five cycles each C-rate.

2.5. Theoretical calculation

To explore the interaction mechanism of functional SiO_2-AM coat and liquid electrolyte, the binding energies and average interaction energy among the imide group, solvent and lithium-ion, were calculated with DFT implemented in Material Studio 2018 software. To make the computational cost affordable, the basic repeat unit of $(AM)_n$, n is 1 or 2, respectively, was used to represent SiO_2-AM. And EC was selected as the single solvent. The Dmol3 module and GGA-PBE function were used to optimize all structures on the basis of DSPP method and DNP base group level and DFT-D modification. The orbital truncation radius was set as 4.6 Å, and the closed shell was selected to calculate the electron energy of the entire structure. The convergence criteria are as follows: the maximum energy variation is 10^{-5} Hartree, the maximum force is 0.002 Hartree/Å, and the maximum displacement is 0.005 Å.

The corresponding binding energies were calculated by the following formula: $E_b = E_{complex} - E_{unit} - E_{Li}^+$ where $E_{complex}$ is the energy of the binding complex, E_{unit} is the energy of $(AM)_n$ or EC, and E^+_{Li} is the energy of Li^+. And average interaction energy $\Delta E = (E_{complex} - E^+_{unit,Li} - nE_{EC})/n$, where And $E^+_{unit,Li}$ is the energy of Li^+(unit) and its derivatives, E_{EC} is the energy of EC. Note that all optimizations started with multiple initial guesses of the structure and the most stable ones were saved.

3. Results and discussion

First of all, starting from the SiO_2 particles with uniform particle size and smooth surface synthesized by a Stober method, a facile preparation route of SiO_2-AM particles is conducted as shown in Fig. 1(a), including two steps, hydrolysis of silane and addition reaction of unsaturated bonds. VTMS, a silane coupling agent containing the carbon-carbon double bond, is used as the bridge media. Because it can modify the SiO_2 particles by hydrolysis and then its carbon-carbon double bond can be grafted with acrylamide (AM) monomer. Fig. 1(b and c) and Fig. 1(e and f) depict the morphology of the obtained SiO_2 particles and SiO_2-AM particles. By the ImageJ software analysis for these particles size in Fig. S1, it is found that the size of SiO_2 particles is about 210–220 nm

according to the result in Fig. 1(d), while the size of SiO_2-AM particles is approximately 240 nm in Fig. 1(g). Moreover, it is evident that the surface of SiO_2-AM particles gets roughed and is covered by some distinct products.

According to the TGA curves of these white powders in Fig. 2, there is an obvious loss weight phenomena for all samples. This can be divided into two sections: below and above 200 °C. As a result, the loss weights of SiO_2, SiO_2-VTMS and SiO_2-AM particles are 8.6%, 3.9% and 5.7% below 200 °C, respectively, which may be resulted from evaporation of water or dehydroxylation. The prepared SiO_2 particles have more hydroxyl groups that would further condense at higher temperatures and behave maximum weight loss below 200 °C. While during the temperature range of 200–550 °C, the loss weights of these samples are 3.1%, 3.6% and 21.7%, respectively. It could be a reason that thermal cracking of carbon chains. The loss weight of SiO_2-AM powder sample containing a thick AM modified layer is the most. Additionally, the color of SiO_2-AM power sample changes to black after heating up to 550 °C, whereas SiO_2-VTMS powder became brown and SiO_2 powder remained be white. All these results illustrate various modified layer of carbon chains for SiO_2, SiO_2-VTMS and SiO_2-AM ceramic particles. Thereby, a series of spectroscopic analyses have been performed to figure out the surface chemical state of the SiO_2-AM particles.

FTIR spectroscopy is a strong and convenient tool to analyze chemical composition of substrate, which is well applicated in our system. The FTIR results of SiO_2 particles and SiO_2-AM particles are shown in Fig. 3(a and b). It is easily observed that some characteristic peaks correspond to the typical chemical bond from SiO_2 and acrylamide, respectively. Fig. 3(a) depicts the whole FTIR spectra in the wavenumber ranging from 400 cm^{-1} to 4000 cm^{-1}. There are the characteristic absorption bands of at 3500-3600 cm^{-1}, 2800-3000 cm^{-1}, 1400-1700 cm^{-1} and 1000-1100 cm^{-1}, which are originated from the N–H, C–H, C–C, $–CONH_2$ and -Si-O functional groups, respectively. Besides, the peaks of 1400–1700 cm^{-1} in Fig. 3(b) are distinguished by amide I, amide II and amide III of SiO_2-AM particles. Meantime, as exhibited in

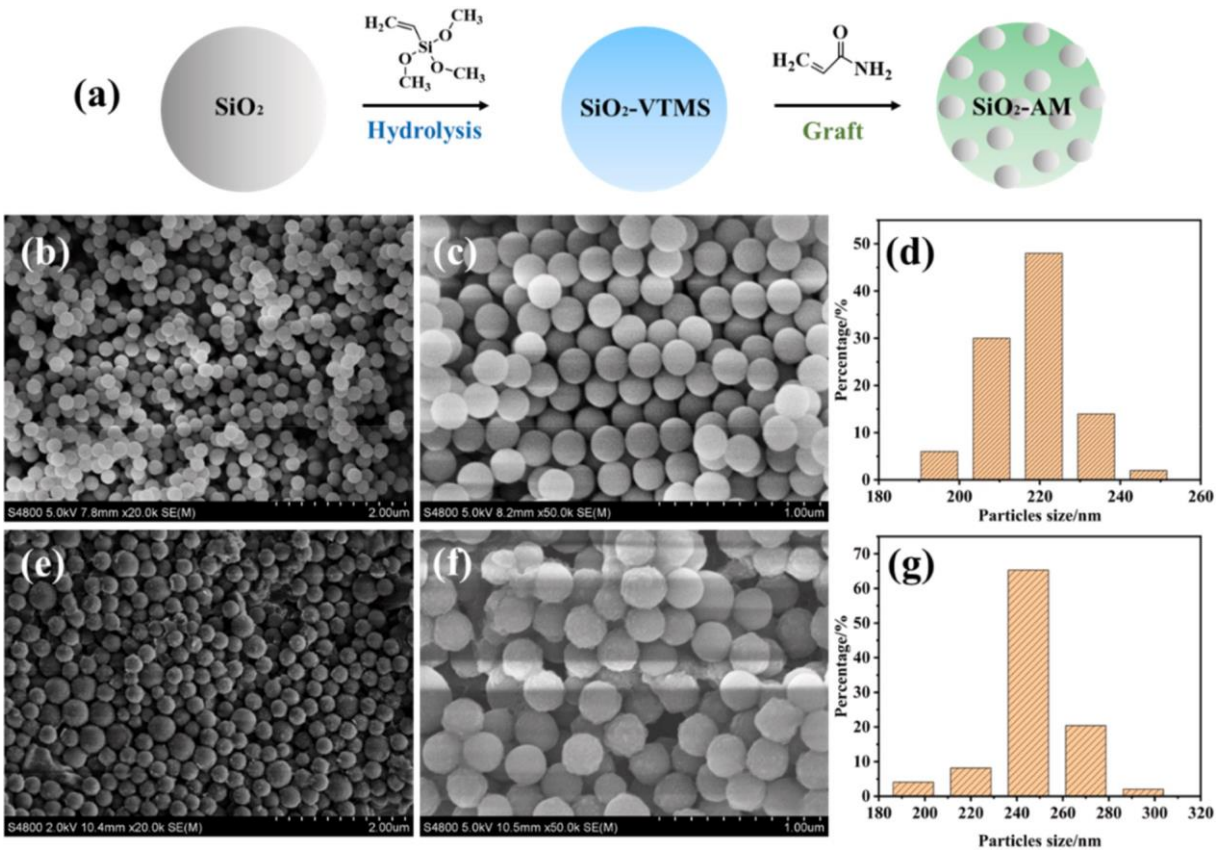

Fig. 1. Schematics of preparation for SiO_2-AM particles (a), morphology (b, c) and particles size analysis (d) of SiO_2 particles, and morphology (e, f) and particles size analysis (g) of SiO_2-AM particles.

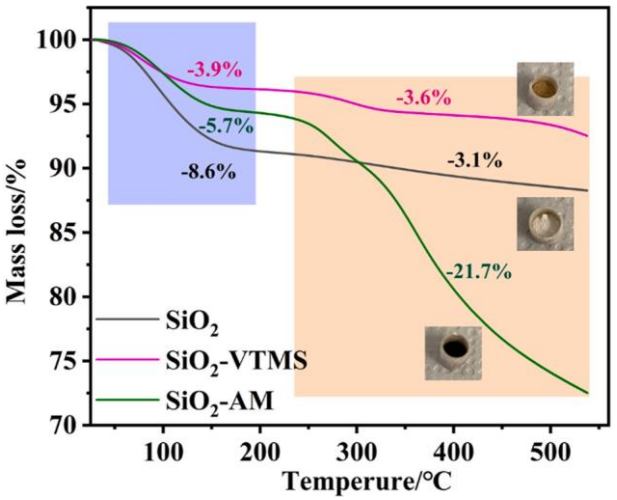

Fig. 2. TGA curves of SiO_2, SiO_2-VTMS and SiO_2-AM particles.

Fig. 3(c), a typical N 1s peak at the binding energy of 399 eV is only observed in the case of SiO_2-AM particles when compared with SiO_2 particles and SiO_2-VTMS particles.

Besides, according to the UV–Vis–NIR spectrum of these particles in Fig. 3(d), it is obvious that SiO_2 has absorption approximately at the wavelength of 300 nm while AM has absorption at the wavelength range of 1500–1800 nm. The synthesized SiO_2-AM particles have all these characteristics from SiO_2 and AM, respectively. Therefore, it is concluded that AM is successfully modified onto the surface of SiO_2. We have prepared the PE/SiO_2 composite separator and the PE/SiO_2-AM composite separator by a blade coating process, respectively. The cross-sectional SEM image in Fig. S2 obviously exhibits a SiO_2-AM layer and porous base film. Compared with pure PE separator, the (110) and (200) peaks of the WAXD profiles of the PE/SiO_2-AM composite ceramic separator in Fig. S3 gradually move to a smaller scattering angle and the intensity of these peaks is weak. The ceramic coating has a low crystallinity or a high proportion of the amorphous phase, which would be quickly permeated by liquid electrolyte. In addition, it is observed from Fig. S4 that the mapping images of Si, O, N and C elements are also dispersed on the surface of the prepared PE/SiO_2-AM composite separator.

In order to evaluate the surface property of PE separator, PE/SiO_2 composite separator and PE/SiO_2-AM composite separator, the contact angle test is performed and shown in Fig. 4(a-c). When using water as testing liquid, PE/SiO_2-AM composite separator displays the lowest contact angle (5°), mainly resulted from stronger hydrophilicity of AM modified layer for SiO_2-AM particles. The contact angles of PE/SiO_2 composite separator and bare PE separator are 56° and 112°, respectively. In the case of organic electrolyte, both the contact angles of PE/SiO_2-AM and PE/SiO_2 composite separators is 0°, lower than 40° of PE separator in Fig. 4(d-f). This is in accordance with some previous reported literatures [36,58]. The improved affinity is majorly resulted from stronger absorption effect between polar oxygen-containing functional group of the ceramic coat and electrolyte molecules for overcoming itself surface tension, and leading to an enhanced wettability. Therefore, we have also explored the wettability of these separators. As expected, the result listed in Table S1 demonstrates that PE/SiO_2-AM composite separator has the highest electrolyte uptake (278%) when compared with PE separator (139%) and PE/SiO_2 composite separator (173%). Additionally, the thermal dimensional stability of these separators is evaluated as well. Samples with the same diameter (1.9 cm)

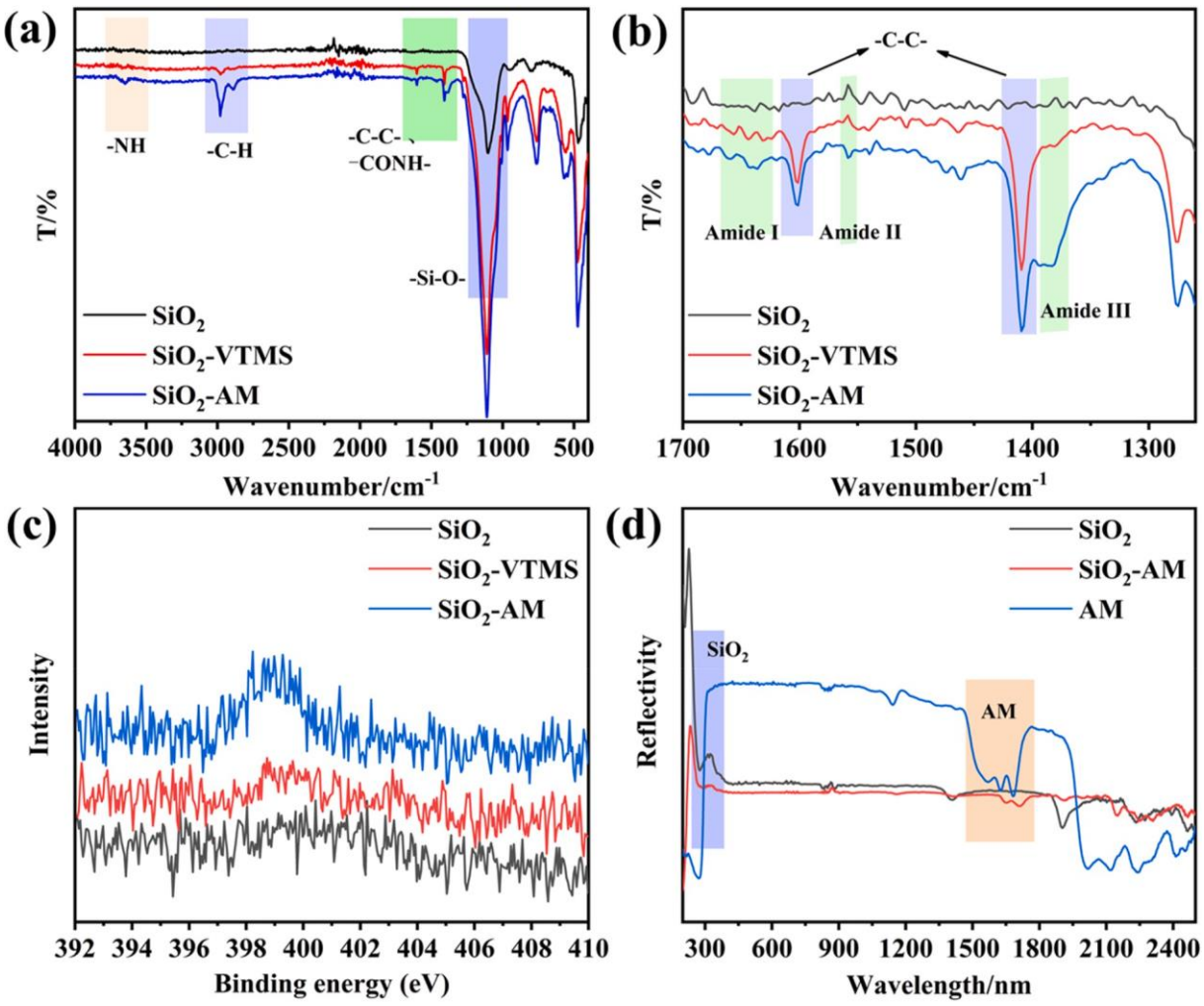

Fig. 3. FTIR (a, b), XPS (c), UV–Vis–NIR (d) of different ceramic particles.

were put them into a drying oven at 135 ˚C or 150 ˚C for 30 min. The image of size shrinkage for these separators after thermal treatment is in Fig. 4(g) and Fig. S5. It could be seen that the size of PE separator is decreased to 81.9% and gets transparent for melt at higher temperature, evincing better dimensional stability of these two ceramic composite separators. As a result, the ceramic coat can play a role of "armour" in preventing the shrinkage of PE matrix.

When located between two electrodes, the separator will affect the contact interface and determine the ion transporting process [59,60]. Therefore, in the light of Nyquist plots and I-t curves in Fig. 5, the transference number of lithium-ion t^{+}_{Li} were calculated using the equation in experimental section and the fitted data is presented in Table 1. The t^{+}_{Li} of PE separator is 0.31, which is lower than 0.43 of PE/SiO_2 composite separator and 0.44 of PE/SiO_2-AM composite separator. This is due to the fact that the ceramic composite separators are able to store more liquid electrolyte and form more channels for ions. Moreover, the interaction can be enhanced between polar group and lithium ions. The SiO_2-AM with polar imide group including C⁻O and N–H bonds provide high-concentration functional sites for a stronger induction effect with lithium ion, which are used to promote the ion selectivity of separator. In brief, PE/SiO_2-AM composite separator exhibits high-performance of transporting lithium-ion because of the charged property and the improved affinity to liquid electrolyte (Fig. 4). We also have investigated different cell configurations by impedance spectroscopy and LSV as depicted in Fig. 6.

is suggested that all separators have good electrochemical stability below 4.5 V, which the voltage applied to the $LiCoO_2$/Li cell. The Nyquist plot of the Li/Li cells in Fig. 6(b) show a large semicircle and a little tail, which mainly represents the charge transfer process at the interface of separator/liquid electrolyte/lithium anode. The $LiCoO_2$/Li cells in Fig. 6(c), there is a semicircle and a slanted line, demonstrating the charge transfer process and solid phase migration process of lithium ions. The Nyquist plots in Fig. 6(b and c) suggests that the cell with PE/ SiO_2-AM composite separator has a decreased charge transfer imped- ance when compared with those cells containing PE separator and PE/ SiO_2 composite separator. The functional ceramic coating facilitates stable transport of lithium ions at the interface of separator/lithium anode. Besides, it is easily seen that all the charge transfer impedances of

Fig. 6(a) displays LSV curves of SS/Li cell with different separators. It

Li/Li cells shown in Fig. S6 are increased with the storing time, importantly, the Li-symmetric cells employing the SiO_2-AM composite separator have the smallest impedance all the time. Fig. 7 shows the schematics of the Li^+ distributing at the interface of composite separator and lithium anode, and an enhanced capacitance of electric double layer (C_d). When ceramic particles such as SiO_2 or Al_2O_3 are introduced, the charge and electric field associated with the particles interact with ion species in the liquid electrolyte, leading to the formation of a double layer or space charge [61]. The space charge layer can promote the conduction of Li^+ [62]. Under the impact of AM modified layer, more lithium ions can be evenly distributed at this interface, according to the capacitive reactance formula of $X_c = 1/(2\pi C_d)$, this situation is in favor of lithium-ion transporting. In addition, it is also attributed to the fact

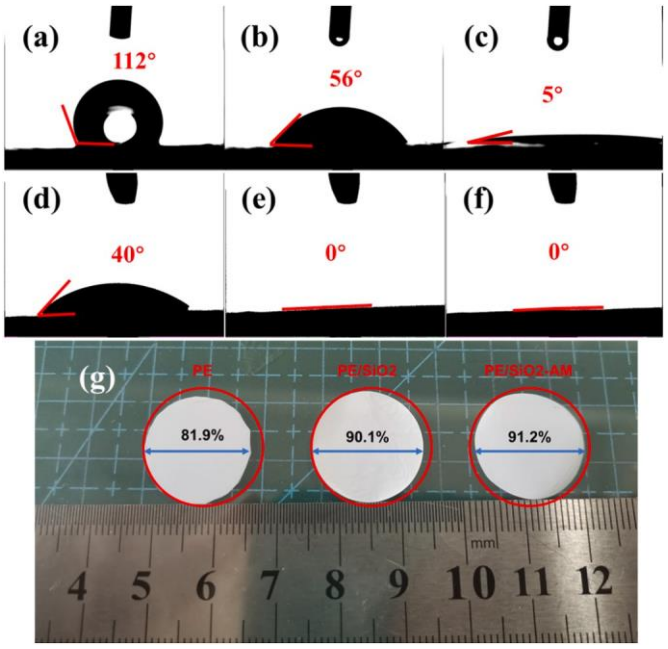

Fig. 4. Contact angle of PE separator (a, d), PE/SiO_2 composite separator (b, e) and PE/SiO_2-AM composite separator (c, f), respectively. Separator shrinkage after thermal treatment at 135 °C for 30 min (g) of PE separator, PE/SiO_2 composite separator and PE/SiO_2-AM composite separator.

that the interface of separator coating and lithium metal anode could be more wettable for liquid electrolyte than that of PE separator matrix and lithium metal anode.

To analyze the interaction between the liquid electrolyte and the SiO_2-AM coat at the molecular level, density functional theory (DFT) calculations were also carried out, and its results is shown in Fig. 8. It could be seen that the binding energies of EC, SiO_2-AM_1, and SiO_2-AM_2 with the lithium-ion are —2.24 eV, —3.32 eV, and —5.50 eV, respectively. Because lithium-ion with positive charge property have strong ability to polarize molecules, which will attract electron-rich species such as O and N atoms in the system [54]. In our calculation, the O atom of imide group will be firstly binding with lithium-ion for effectively reducing more energy of the entire system. In addition, SiO_2 modified with more repeated units of AM, can adsorb more lithium-ions, and this binding structure will be more stable, which prompt lithium-ions distributing at the interface between lithium anode and electrolyte. It is generally believed that lithium-ion is able to interact with four EC molecular [63]. Therefore, we continue to discuss the interaction with other EC molecular after lithium-ion cooperating with SiO_2-AM and calculate these binding energies (Figs. S7–S9). As exhibited in Table 2,

Table 1
The lithium-ion transference number of PE separator and composite separators.

Separators	I_0/μA	I_s/μA	R_0/Ω	R_s/Ω	t_{Li+}
PE	44.1	38.0	105.4	106.4	**0.31**
PE/SiO_2	44.6	36.5	102.3	97.1	**0.43**
PE/SiO_2-AM	64.5	55.0	67.8	68.91	**0.44**

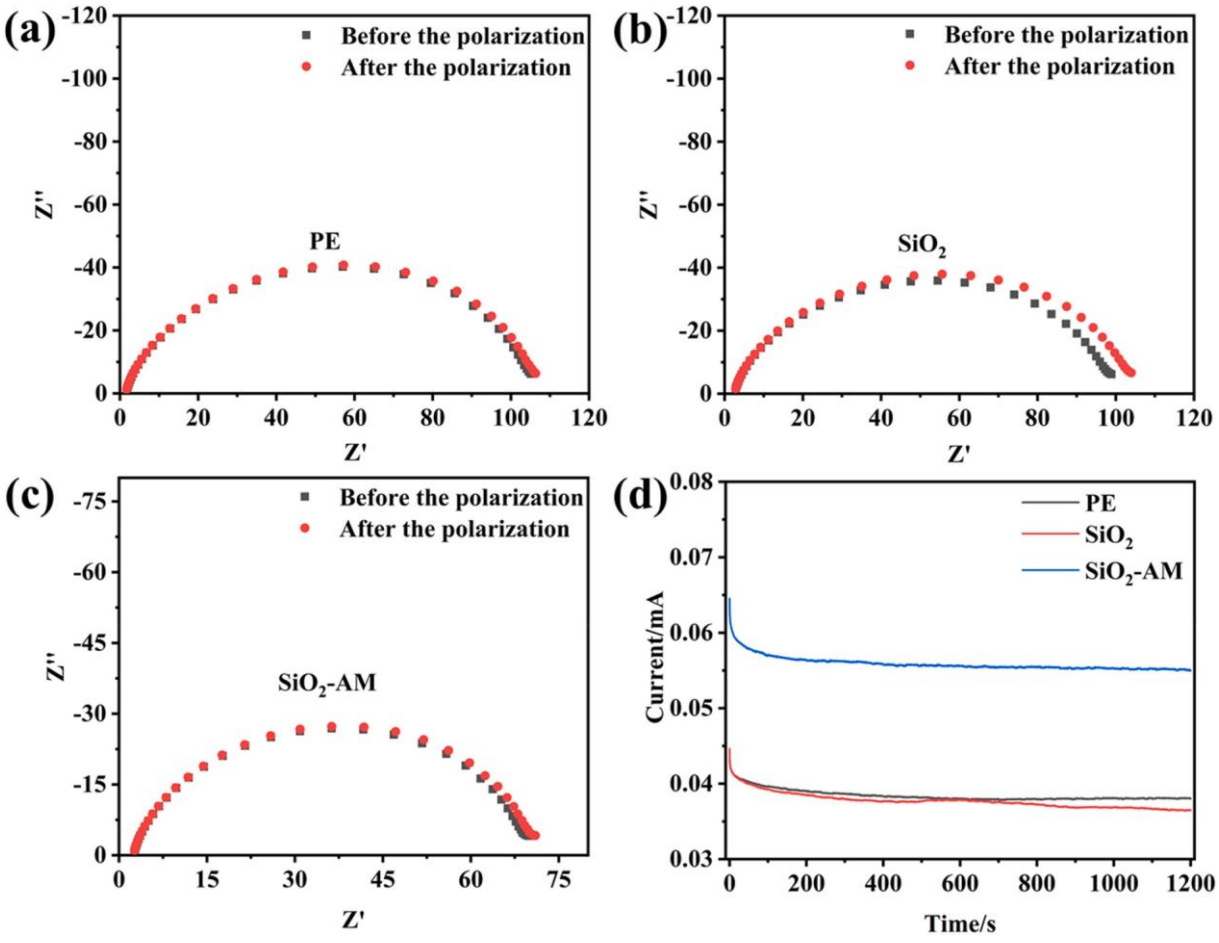

Fig. 5. Nyquist plots of (a) PE separator, (b) PE/SiO_2 composite separator and (c) PE/SiO_2-AM composite separator, before and after the polarization; (d) Constant potential polarization curves of Li/Li cell based on different separators.

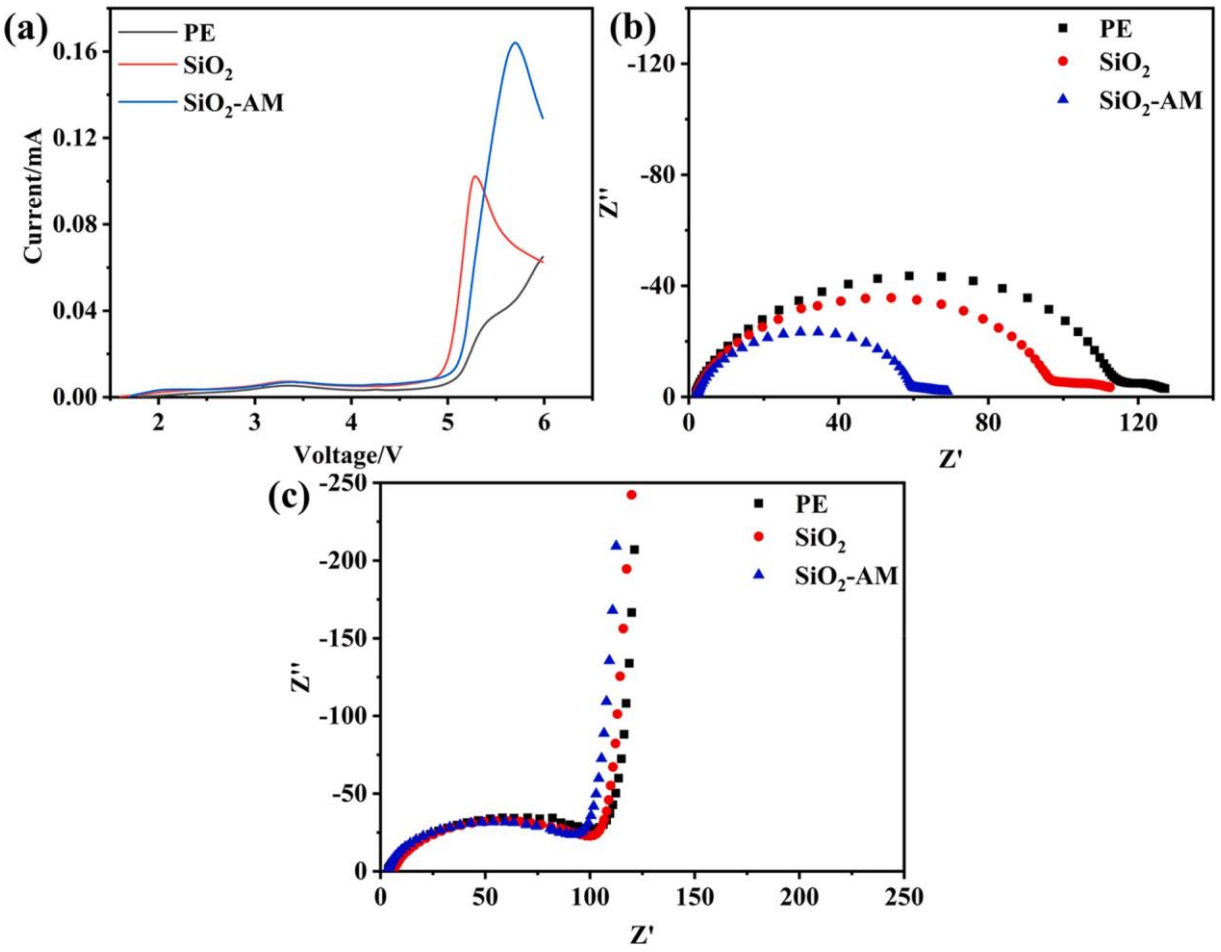

Fig. 6. LSV of SS/Li cell (a) and Nyquist plots of Li/Li cell (b) and $LiCoO_2$/Li cell (c) containing different separators.

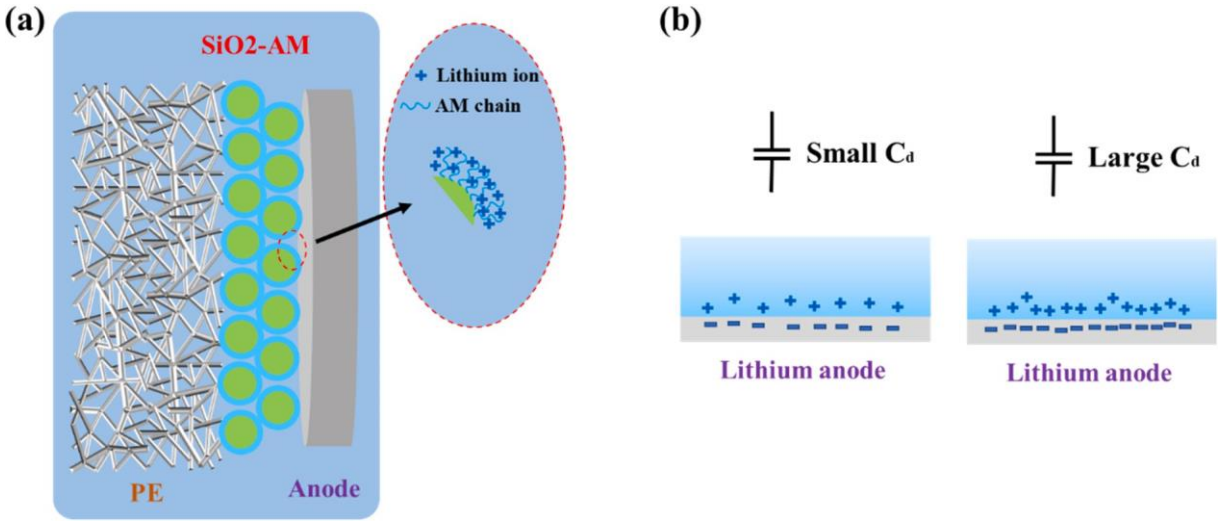

Fig. 7. Schematics for lithium-ion distributing at the interface of separator and lithium anode.

when lithium-ion relating to four EC molecular one by one, the average interaction energies are —2.24 eV, —1.97 eV, —1.68 eV and —1.33 eV, respectively. While in the case of SiO_2-AM_1, after binding with lithium-ion, the average interaction energies with EC molecular are —1.70 eV, —1.33 eV and —1.12 eV, respectively. This illustrates that the amide group can effectively reduce the interaction between lithium ion and the solvent EC, which will make it easier to desolvation. Especially for SiO_2-AM_2, have lower average interaction energies of —1.05 eV and —0.84 eV to EC molecular. In brief, negative properties of imide group is beneficial to stabilize the interface of electrode/electrolyte and facilitate lithium-ion transport.

In order to evaluate the performance of these different separators faced with Li metal anode, nonblocking Li-symmetric testing system has been carried out by galvanostatic stripping/deposition cycles. The Li-

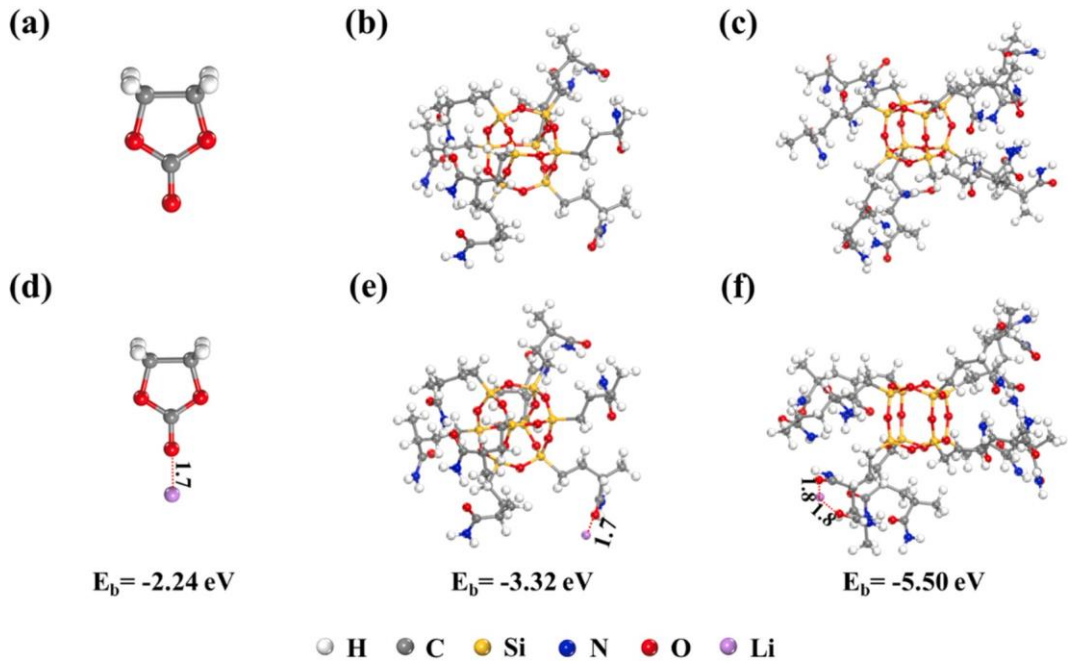

Fig. 8. Result of density functional theory (DFT) calculations, the optimized structure of EC (a), SiO_2-AM_1 (b), SiO_2-AM_2 (c); and the interaction between lithium ion and EC (d), SiO_2-AM_1 (e), SiO_2-AM_2 (f), respectively.

Table 2
Interaction among different species.

Interaction Unit	unit-Li^+	Li^+(unit)-EC	Li^+(unit)-2EC	Li^+(unit)-3EC
EC	—2.24 eV	—1.97 eV	—1.68 eV	—1.33 eV
SiO_2-$(AM)_1$	—3.32 eV	—1.70 eV	—1.33 eV	—1.12 eV
SiO_2-$(AM)_2$	—5.50 eV	—1.05 eV	—0.84 eV	

symmetric cells with PE separator, PE/SiO_2 composite separator and PE/SiO_2-AM composite separator were firstly cycled at a current density of 0.75 mA cm^{-2} (the areal capacity was 0.75 mAh cm^{-2}) and then the surface morphology of these separator was observed after long-term Li stripping/plating cycles. According to the results in Fig. 9(a), the cells containing PE/SiO_2-AM composite separator have the lowest overvoltage of around 50–100 mV, be basically stable during the whole long-term cycles, while the cells with pure PE separator and PE/SiO_2 composite separator performs an increased overpotential (>150 mV) at the latter stage. Besides, Fig. 9(b) shows that the porous structure of PE separator is almost blocked after the repeated lithium stripping/plating cycles, which could result in the increasing overpotential at the latter stage. It is also seen that some by-products have occupied part interspace among the ceramic particles in Fig. 9(c and d). During each lithium deposition process, the corresponding lithium electrode will expand towards the separator for new formed deposition layer (the thickness >$3.64*10^{-4}$ cm calculated by equation (3) in experimental section) [64, 65]. The ceramic coating ($6*10^{-4}$ cm) is able to relieve the expand pressure of lithium electrode to some extent. Meanwhile, we have tested the electrochemical performance of these Li-symmetric cells under the same stripping/deposition capacity (0.75 mAh cm^{-2}) at a charging (stripping) current density of 0.75 mA cm^{-2} for 1 h and a discharging (deposition) current density of 0.15 mA cm^{-2} for 5 h. The related performance results in Fig. S10 and the optical images of Li electrodes in Fig. S11 demonstrate that the surface of deposited lithium at a small current density is shiner surface than that of lithium deposited at a large current density, and this is consistent with previous reports [66].

Fig. 10 shows the performance of $LiCoO_2$/Li half cells containing different separators. All cells are evaluated in a voltage range of 3–4.4 V. The corresponding coulombic efficiency of these cells is almost 99.5%–100% during stable cycling process as depicted in Fig. 10(a). $LiCoO_2$/Li cells assembled with PE separator, PE/SiO_2 composite separator and PE/SiO_2-AM composite separator have the discharge capacity of 119.7 mAh g^{-1}, 119.7 mAh g^{-1} and 136.8 mAh g^{-1} after 100 cycles at a current density of 1 C, respectively. According to the performance comparison Table S2, the electrochemical performance of these half cells is closely related to active material type and load content, liquid electrolyte and testing current. The active material in our experiment had the highest load and so actual testing current is the highest. Fig. 10(a) and Fig. S12 indicates that the cell containing PE/SiO_2-AM composite separator exhibits great cycling stability and higher discharge capacity. This could be resulted from better interface compatibility among the composite separator, liquid electrolyte and lithium metal anode. On the other hand, it is also important for separator to take in sufficient liquid electrolyte, because it is continuously consumed in the Li-deposited process. To study the variation about the surface of separator furtherly, these used separator are taken for XPS characterization. It can be seen in Fig. S13 that the surface of all separator toward Li metal anode has lithium source signal, which could be resulted from dead Li or adherent SEI component. From binding energy, adherent SEI component should be higher than dead Li. Furthermore, in the case of SiO_2-AM composite separator, the C 1s peak at 291.0 eV gets enhanced, which means the functional AM layer is more conducive to the formation of SEI layer. Fig. 10(b) and Fig. S12 show the rate performance of these cells with different separators. All cells are firstly charged at a current density of 0.2C and discharged for 5 cycles at the current densities of 0.2C, 0.5C, 1 C, 2 C and 3 C, respectively. As expected, the cells with the composite separators show higher discharge capacity than that of the cell using PE separator. After the rate performance tests, electrochemical impedance spectra were collected. The Nyquist plots of the cells with PE/SiO_2-AM composite separator (Fig. S14) show the lowest impedance, demonstrating the superior compatibility with liquid electrolyte.

4. Conclusion

In this study, SiO_2 particles with polar amide groups were coated onto the surface of PE separator. The obtained PE/SiO_2-AM composite separator has stronger affinity of electrolyte at room temperature and

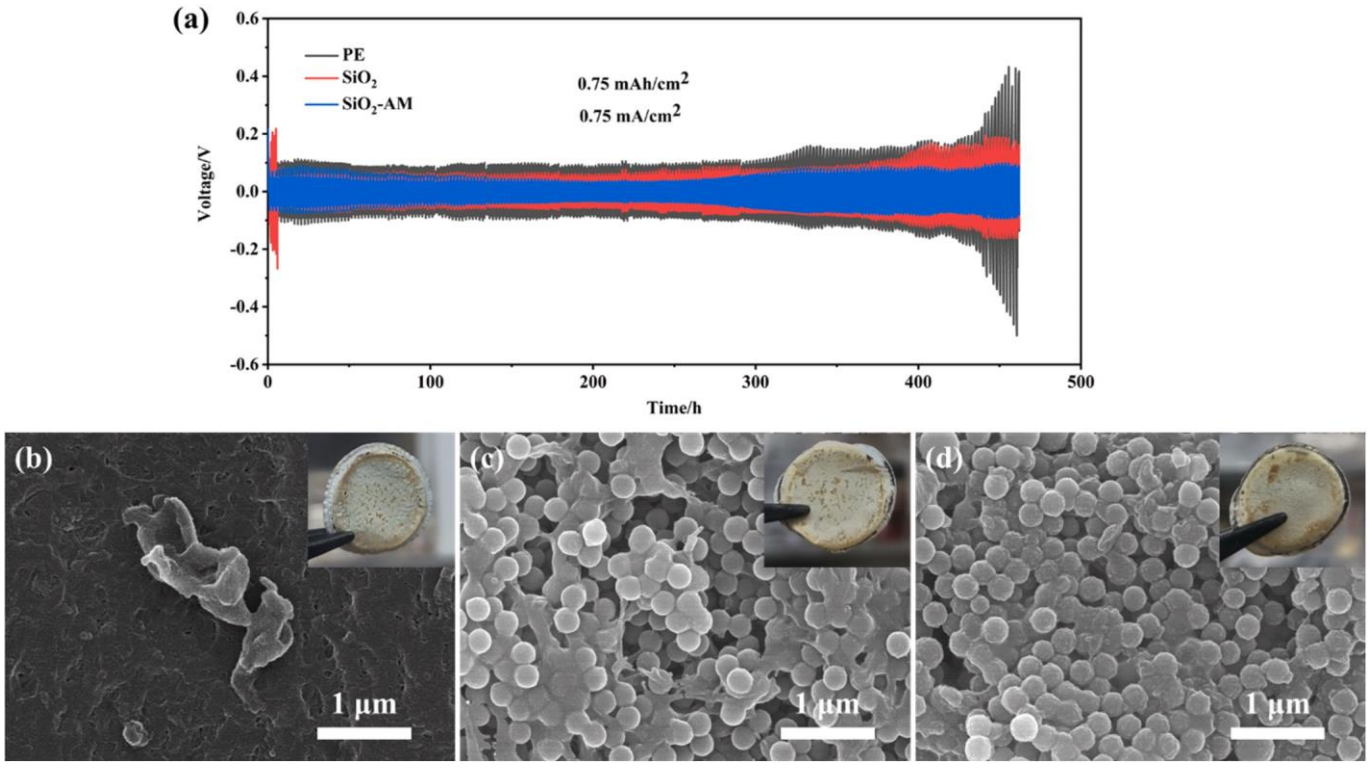

Fig. 9. Cycling stability of Li/Li cells with the different separators (a) and surface morphology after 200 cycles of PE separator (b), PE/SiO_2 composite separator (c) and PE/SiO_2-AM composite separator (d).

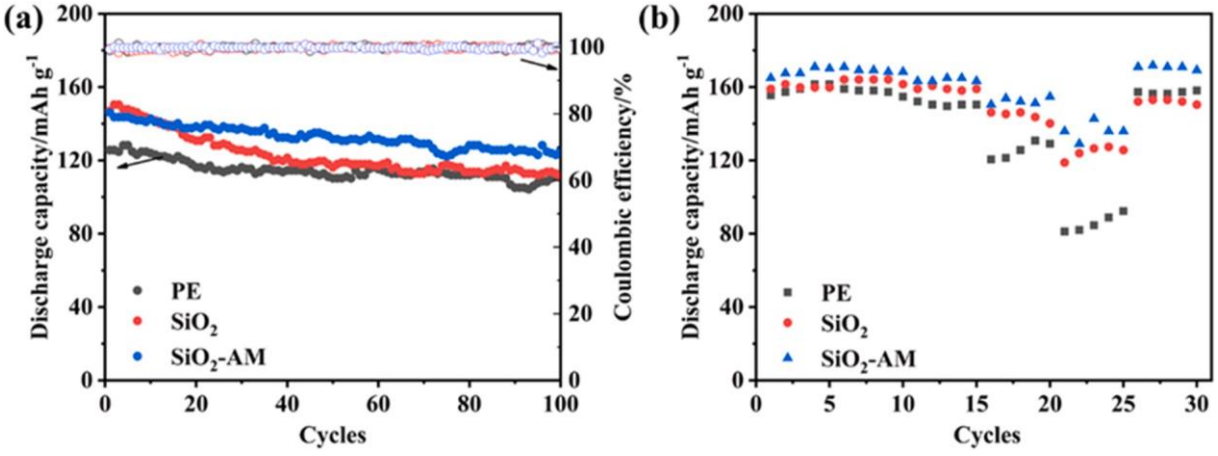

Fig. 10. Battery performance of $LiCoO_2$/Li cells based on different separators, (a) cycle performance, and (b) rate performance.

better thermal stability at high temperature. This composite separator still be stable below 4.5 V (vs. Li/Li^+) and has an improved lithium-ion transference number of 0.44. After assembling the battery, it confirms that PE/SiO_2-AM composite separator can regulate the lithium-ion transport property and increase the capacity retention of their cells. Therefore, our results reveal that functional composite coat would be a promising battery component for enhancing battery safety while main- taining the cycling performance of lithium-based battery employing conventional polyolefin separator and liquid electrolyte.

CRediT authorship contribution statement

Lei Sheng: Experiments, writing original draft. **Xin Xie:** Software, Investigation. **Catia Arbizzani:** Conceptualization, review and editing. **Luca Bargnesi:** Characterization of samples, data collection. **Yaozong Bai:** Research funding. **Gaojun Liu:** Administration, review and editing. **Haoyu Dong:** Review and editing. **Tao Wang:** Analysis of data, review and editing. **Jianping He:** Supervision, review and editing.

Declaration of competing interest

The authors declare that they have no known competing financial interests or personal relationships that could have appeared to influence the work reported in this paper.

Acknowledgements

The author was grateful for the financial support from the financial support from the Fundamental Research Funds for the Central Universities (NE2018104), the National Natural Science Foundation of China

(11575084) and A Project Funded by the Priority Academic Program Development of Jiangsu Higher Education Institutions (PAPD). Italian Ministry of Economic Development and ENEA PTR 2019–2021 project and China Scholarship Council (CSC) are also acknowledged.

Appendix A. Supplementary data

Supplementary data to this article can be found online at XXXXXXXX

References

[1] Y. Li, J. Zhu, R. Shi, M. Dirican, P. Zhu, C. Yan, H. Jia, J. Zang, J. He, X. Zhang, Ultrafine and polar ZrO_2-inlaid porous nitrogen-doped carbon nanofiber as efficient polysulfide absorbent for high-performance lithium-sulfur batteries with long lifespan, Chem. Eng. J. 349 (2018) 376–387, https://doi.org/10.1016/j.cej.2018.05.074.

[2] W. Luo, S. Cheng, M. Wu, X. Zhang, D. Yang, X. Rui, A review of advanced separators for rechargeable batteries, J. Power Sources 509 (2021), 230372, https://doi.org/10.1016/j.jpowsour.2021.230372230372.

[3] P. Zhai, K. Liu, Z. Wang, L. Shi, S. Yuan, Multifunctional separators for high-performance lithium ion batteries, J. Power Sources 499 (2021), 229973, https://doi.org/10.1016/j.jpowsour.2021.229973229973.

[4] Y. Pan, S. Chou, H.K. Liu, S.X. Dou, Functional membrane separators for next-generation high-energy rechargeable batteries, Natl. Sci. Rev. 4 (2017) 917–933, https://doi.org/10.1093/nsr/nwx037917.

[5] W. Cai, Y. Yao, G. Zhu, C. Yan, L. Jiang, C. He, J. Huang, Q. Zhang, A review on energy chemistry of fast-charging anodes, Chem. Soc. Rev. 49 (2020) 3806–3833, https://doi.org/10.1039/C9CS00728H3806.

[6] L. Ding, C. Zhang, T. Wu, F. Yang, F. Lan, Y. Cao, M. Xiang, Effect of temperature on compression behavior of polypropylene separator used for lithium-ion battery, J. Power Sources 466 (2020), 228300, https://doi.org/10.1016/j.jpowsour.2020.228300228300.

[7] C. Zhao, T. Wang, Z. Huang, J. Wu, H. Zhou, M. Ma, J. Xu, Z. Wang, H. Li, J. Sun, Q. Wang, Experimental study on thermal runaway of fully charged and overcharged lithium-ion batteries under adiabatic and side-heating test, J. Energy Storage 38 (2021), 102519, https://doi.org/10.1016/j.est.2021.102519102519.

[8] D.H. Jeon, S.M. Baek, Thermal modeling of cylindrical lithium ion battery during discharge cycle, Energy Convers. Manag. 52 (2011) 2973–2981, https://doi.org/10.1016/j.enconman.2011.04.0132973.

[9] M. Yanilmaz, Y. Lu, J. Zhu, X. Zhang, Silica/polyacrylonitrile hybrid nanofiber membrane separators via sol-gel and electrospinning techniques for lithium-ion batteries, J. Power Sources 313 (2016) 205–212, https://doi.org/10.1016/j.jpowsour.2016.02.089.

[10] J. Zhu, E. Yildirim, K. Aly, J. Shen, C. Chen, Y. Lu, M. Jiang, D. Kim, A.E. Tonelli, M.A. Pasquinelli, P.D. Bradford, X. Zhang, Hierarchical multi-component nanofiber separators for lithium polysulfide capture in lithium–sulfur batteries: an experimental and molecular modeling study, J. Mater. Chem. 4 (2016) 13572–13581, https://doi.org/10.1039/C6TA04577D.

[11] Z. Wang, L. Shen, S. Deng, P. Cui, X. Yao, 10 μm-Thick high-strength solid polymer electrolytes with excellent interface compatibility for flexible all-solid-state lithium-metal batteries, Adv. Mater. 33 (2021), 2100353, https://doi.org/10.1002/adma.202100353.

[12] C. Martinez-Cisneros, C. Antonelli, B. Levenfeld, A. Varez, J. Sanchez, Evaluation of polyolefin-based macroporous separators for high temperature Li-ion batteries, Electrochim. Acta 216 (2016) 68–78, https://doi.org/10.1016/j.electacta.2016.08.10568.

[13] C. Zhang, H. Li, S. Wang, Y. Cao, H. Yang, X. Ai, F. Zhong, A polyethylene microsphere-coated separator with rapid thermal shutdown function for lithium-ion batteries, J. Energy Chem. 44 (2020) 33–40, https://doi.org/10.1016/j.jechem.2019.09.01733.

[14] J. Choi, S.H. Kim, D. Kim, Enhancement of thermal stability and cycling performance in lithium-ion cells through the use of ceramic-coated separators, J. Power Sources 195 (2010) 6192–6196, https://doi.org/10.1016/j.jpowsour.2009.11.0206192.

[15] M. Kim, G.Y. Han, K.J. Yoon, J.H. Park, Preparation of a trilayer separator and its application to lithium-ion batteries, J. Power Sources 195 (2010) 8302–8305, https://doi.org/10.1016/j.jpowsour.2010.07.0168302.

[16] S.H. Yoo, C.K. Kim, Enhancement of the meltdown temperature of a lithium ion battery separator via a nanocomposite coating, Ind. Eng. Chem. Res. 48 (2009) 9936–9941, https://doi.org/10.1021/ie901141u9936.

[17] J. Park, J. Cho, W. Park, D. Ryoo, S. Yoon, J.H. Kim, Y.U. Jeong, S. Lee, Close-packed SiO_2/poly(methyl methacrylate) binary nanoparticles-coated polyethylene separators for lithium-ion batteries, J. Power Sources 195 (2010) 8306–8310, https://doi.org/10.1016/j.jpowsour.2010.06.1128306.

[18] H. Jeong, S. Lee, Closely packed SiO_2 nanoparticles/poly(vinylidene fluoride-hexafluoropropylene) layers-coated polyethylene separators for lithium-ion batteries, J. Power Sources 196 (2011) 6716–6722, https://doi.org/10.1016/j.jpowsour.2010.11.0376716.

[19] R. Juang, C. Hsieh, P. Chen, Y. Chen, Microwave-assisted synthesis of titania coating onto polymeric separators for improved lithium-ion battery performance, J. Power Sources 286 (2015) 526–533, https://doi.org/10.1016/j.jpowsour.2015.04.023526.

[20] K. Peng, B. Wang, Y. Li, C. Ji, Magnetron sputtering deposition of TiO_2 particles on polypropylene separators for lithium-ion batteries, RSC Adv. 5 (2015) 81468–81473, https://doi.org/10.1039/c5ra18171b81468.

[21] X. Zhu, X. Jiang, X. Ai, H. Yang, Y. Cao, TiO_2 ceramic-grafted polyethylene separators for enhanced thermostability and electrochemical performance of lithium-ion batteries, J. Membr. Sci. 504 (2016) 97–103, https://doi.org/10.1016/j.memsci.2015.12.05997.

[22] L. Liu, Y. Wang, C. Gao, C. Yang, K. Wang, H. Li, H. Gu, Ultrathin ZrO_2-coated separators based on surface sol-gel process for advanced lithium ion batteries, J. Membr. Sci. 592 (2019), 117368, https://doi.org/10.1016/j.memsci.2019.117368117368.

[23] X. Luo, Y. Liao, Y. Zhu, M. Li, F. Chen, Q. Huang, W. Li, Investigation of nano-CeO_2 contents on the properties of polymer ceramic separator for high voltage lithium ion batteries, J. Power Sources 348 (2017) 229–238, https://doi.org/10.1016/j.jpowsour.2017.02.085229.

[24] T. Lee, W. Kim, Y. Lee, M. Ryou, Y.M. Lee, Effect of Al_2O_3 coatings prepared by RF sputtering on polyethylene separators for high-power lithium ion batteries, Macromol. Res. 22 (2014) 1190–1195, https://doi.org/10.1007/s13233-014-2163-11190.

[25] M. Kim, J.H. Park, Inorganic thin layer coated porous separator with high thermal stability for safety reinforced Li-ion battery, J. Power Sources 212 (2012) 22–27, https://doi.org/10.1016/j.jpowsour.2012.03.03822.

[26] H. Jeon, S.Y. Jin, W.H. Park, H. Lee, H. Kim, M. Ryou, Y.M. Lee, Plasma-assisted water-based Al_2O_3 ceramic coating for polyethylene-based microporous separators for lithium metal secondary batteries, Electrochim. Acta 212 (2016) 649–656, https://doi.org/10.1016/j.electacta.2016.06.172649.

[27] W. Na, K.H. Koh, A.S. Lee, S. Cho, B. Ok, S. Hwang, J.H. Lee, C.M. Koo, Binder-less chemical grafting of SiO_2 nanoparticles onto polyethylene separators for lithium-ion batteries, J. Membr. Sci. 573 (2019) 621–627, https://doi.org/10.1016/j.memsci.2018.12.039621.

[28] X. Wei, Q. Wang, Z. Song, Z. Yue, T. Tian, C. Yin, L. Zhou, X. Li, Effect of hydroxyls and particle size on the electrochemical performance of boehmite coated PE separators for lithium-ion batteries, Solid State Ionics 366–367 (2021), 115652, https://doi.org/10.1016/j.ssi.2021.115652115652.

[29] P. Zhang, L. Chen, C. Shi, P. Yang, J. Zhao, Development and characterization of silica tube-coated separator for lithium ion batteries, J. Power Sources 284 (2015) 10–15, https://doi.org/10.1016/j.jpowsour.2015.02.12610.

[30] Y.B. Kim, T. Tran-Phu, M. Kim, D. Jung, G. Yi, J.H. Park, Facilitated ion diffusion in multiscale porous particles: application in battery separators, ACS Appl. Mater. Interfaces 7 (2015) 4511–4517, https://doi.org/10.1021/am506797d.

[31] J.H. Ahn, H. Kim, Y. Lee, D. Esken, D. Dehe, H.A. Song, D. Kim, Nanostructured reactive alumina particles coated with water-soluble binder on the polyethylene separator for highly safe lithium-ion batteries, J. Power Sources 506 (2021) 230119, https://doi.org/10.1016/j.jpowsour.2021.230119230119.

[32] W. Fu, R. Xu, X. Zhang, Z. Tian, H. Huang, J. Xie, C. Lei, Enhanced wettability and electrochemical performance of separators for lithium-ion batteries by coating core-shell structured silica-poly(cyclotriphosphazene-co-4,4'-sulfonyldiphenol) particles, J. Power Sources 436 (2019), 226839, https://doi.org/10.1016/j.jpowsour.2019.226839226839.

[33] J. Cho, Y. Jung, Y.S. Lee, D. Kim, High performance separator coated with amino-functionalized SiO_2 particles for safety enhanced lithium-ion batteries, J. Membr. Sci. 535 (2017) 151–157, https://doi.org/10.1016/j.memsci.2017.04.042151.

[34] H. Zhang, L. Sheng, Y. Bai, S. Song, G. Liu, H. Xue, T. Wang, X. Huang, J. He, Amino-functionalized Al_2O_3 particles coating separator with excellent lithium-ion transport properties for high-power density lithium-ion batteries, Adv. Eng. Mater. 22 (2020), 1901545, https://doi.org/10.1002/adem.2019015451901545.

[35] W. Na, A.S. Lee, J.H. Lee, S.S. Hwang, E. Kim, S.M. Hong, C.M. Koo, Lithium dendrite suppression with UV-curable polysilsesquioxane separator binders, ACS Appl. Mater. Interfaces 8 (2016) 12852–12858, https://doi.org/10.1021/acsami.6b0273512852.

[36] C. Shi, P. Zhang, L. Chen, P. Yang, J. Zhao, Effect of a thin ceramic-coating layer on thermal and electrochemical properties of polyethylene separator for lithium-ion batteries, J. Power Sources 270 (2014) 547–553, https://doi.org/10.1016/j.jpowsour.2014.07.142547.

[37] R. Xu, L. Sheng, H. Gong, Y. Kong, Y. Yang, M. Li, Y. Bai, S. Song, G. Liu, T. Wang, X. Huang, J. He, High-performance Al_2O_3/PAALi composite separator prepared by water-based slurry for high-power density lithium-based battery, Adv. Eng. Mater. 23 (2021), 2001009, https://doi.org/10.1002/adem.2020010092001009.

[38] Y.S. Jung, A.S. Cavanagh, L. Gedvilas, N.E. Widjonarko, I.D. Scott, S. Lee, G. Kim, S.M. George, A.C. Dillon, Improved functionality of lithium-ion batteries enabled by atomic layer deposition on the porous microstructure of polymer separators and coating electrodes, Adv. Energy Mater. 2 (2012) 1022–1027, https://doi.org/10.1002/aenm.2011007501022.

[39] J. Zhu, C. Chen, Y. Lu, J. Zang, M. Jiang, D. Kim, X. Zhang, Highly porous polyacrylonitrile/graphene oxide membrane separator exhibiting excellent anti-self-discharge feature for high-performance lithium–sulfur batteries, Carbon 101 (2016) 272–280, https://doi.org/10.1016/j.carbon.2016.02.007.

[40] Z. Zhang, L. Wu, D. Zhou, W. Weng, X. Yao, Flexible sulfide electrolyte thin membrane with ultrahigh ionic conductivity for all-solid-state lithium batteries, Nano Lett. 21 (2021) 5233–5239, https://doi.org/10.1021/acs.nanolett.1c01344.

[41] J. Zhu, M. Yanilmaz, K. Fu, C. Chen, Y. Lu, Y. Ge, D. Kim, X. Zhang, Understanding glass fiber membrane used as a novel separator for lithium–sulfur batteries, J. Membr. Sci. 504 (2016) 89–96, https://doi.org/10.1016/j.memsci.2016.01.020.

[42] Z. Wang, Q. Guo, R. Jiang, S. Deng, J. Ma, P. Cui, X. Yao, Porous poly(vinylidene fluoride) supported three-dimensional poly(ethylene glycol) thin solid polymer electrolyte for flexible high temperature all-solid-state lithium metal batteries, Chem. Eng. J. 435 (2022), 135106, https://doi.org/10.1016/j.cej.2022.135106.
[43] Z. Li, A.D. Pauric, G.R. Goward, T.J. Fuller, J.M. Ziegelbauer, M.P. Balogh, I. C. Halalay, Manganese sequestration and improved high-temperature cycling of Li-ion batteries by polymeric aza-15-crown-5, J. Power Sources 272 (2014) 1134–1141, https://doi.org/10.1016/j.jpowsour.2014.04.0731134.
[44] F. Xu, S. Deng, Q. Guo, D. Zhou, X. Yao, Quasi-Ionic liquid enabling single-phase poly(vinylidene fluoride)-based polymer electrolytes for solid-state $LiNi_{0.6}Co_{0.2}Mn_{0.2}O_2$||Li batteries with rigid-flexible coupling interphase, Small Methods 5 (2021), 2100262, https://doi.org/10.1002/smtd.202100262.
[45] G. Liu, J. Shi, M. Zhu, W. Weng, L. Shen, J. Yang, X. Yao, Ultra-thin free-standing sulfide solid electrolyte film for cell-level high energy density all-solid-state lithium batteries, Energy Storage Mater. 38 (2021) 249–254, https://doi.org/10.1016/j.ensm.2021.03.017.
[46] Z. Hao, Y. Wu, Q. Zhao, J. Tang, Q. Zhang, X. Ke, J. Liu, Y. Jin, H. Wang, Functional separators regulating ion transport enabled by metal-organic frameworks for dendrite-free lithium metal anodes, Adv. Funct. Mater. (2021), 2102938, https://doi.org/10.1002/adfm.2021029382102938.
[47] Y. Wen, X. Wang, Y. Yang, M. Liu, W. Tu, M. Xu, G. Sun, S. Kawaguchi, G. Cao, W. Li, Covalent organic framework-regulated ionic transportation for high-performance lithium-ion batteries, J. Mater. Chem. 7 (2019) 26540–26548, https://doi.org/10.1039/C9TA09570E26540.
[48] Z. Chang, Y. Qiao, H. Yang, X. Cao, X. Zhu, P. He, H. Zhou, Sustainable Lithium-Metal Battery Achieved by a Safe Electrolyte Based on Recyclable and Low-Cost Molecular Sieve, Angewandte Chemie International Edition, 2021, https://doi.org/10.1002/anie.202104124.
[49] H. Huo, X. Li, Y. Chen, J. Liang, S. Deng, X. Gao, K. Doyle-Davis, R. Li, X. Guo, Y. Shen, C. Nan, X. Sun, Bifunctional Composite Separator with a Solid-State-Battery Strategy for Dendrite-free Lithium Metal Batteries, Energy Storage Materials, 2019, https://doi.org/10.1016/j.ensm.2019.12.022.
[50] C.Z. Zhao, P.Y. Chen, R. Zhang, X. Chen, B.Q. Li, X.Q. Zhang, X.B. Cheng, Q. Zhang, An ion redistributor for dendrite-free lithium metal anodes, Sci. Adv. 4 (2018), https://doi.org/10.1126/sciadv.aat3446 eaat3446.
[51] X. Han, J. Chen, M. Chen, W. Zhou, X. Zhou, G. Wang, C. Wong, B. Liu, L. Luo, S. Chen, S. Shi, Induction of planar Li growth with designed interphases for dendrite-free Li metal anodes, Energy Storage Mater. 39 (2021) 250–258, https://doi.org/10.1016/j.ensm.2021.04.029250.
[52] Z. Hu, F. Liu, J. Gao, W. Zhou, H. Huo, J. Zhou, L. Li, Dendrite-free lithium plating induced by in situ transferring protection layer from separator, Adv. Funct. Mater. 30 (2019), 1907020, https://doi.org/10.1002/adfm.2019070201907020.
[53] X. Zuo, J. Wu, X. Ma, X. Deng, J. Cai, Q. Chen, J. Liu, J. Nan, A poly(vinylidene fluoride)/ethyl cellulose and amino-functionalized nano-SiO_2 composite coated separator for 5 V high-voltage lithium-ion batteries with enhanced performance, J. Power Sources 407 (2018) 44–52, https://doi.org/10.1016/j.jpowsour.2018.10.05644.
[54] C. Li, S. Liu, C. Shi, G. Liang, Z. Lu, R. Fu, D. Wu, Two-dimensional molecular brush-functionalized porous bilayer composite separators toward ultrastable high-current density lithium metal anodes, Nat. Commun. 10 (2019), https://doi.org/10.1038/s41467-019-09211-z.
[55] X. Li, Y. Liu, Y. Pan, M. Wang, J. Chen, H. Xu, Y. Huang, W.M. Lau, A. Shan, J. Zheng, D. Mitlin, A functional SrF_2 coated separator enabling a robust and dendrite-free solid electrolyte interphase on a lithium metal anode, J. Mater. Chem. 7 (2019) 21349–21361, https://doi.org/10.1039/C9TA06908A21349.
[56] J. Xiao, P. Zhai, Y. Wei, X. Zhang, W. Yang, S. Cui, C. Jin, W. Liu, X. Wang, H. Jiang, Z. Luo, X. Zhang, Y. Gong, In-Situ formed protecting layer from organic/inorganic concrete for dendrite-free lithium metal anodes, Nano Lett. (2020), https://doi.org/10.1021/acs.nanolett.0c01085.
[57] L.E. Camacho-Forero, P.B. Balbuena, Effects of charged interfaces on electrolyte decomposition at the lithium metal anode, J. Power Sources 472 (2020), 228449, https://doi.org/10.1016/j.jpowsour.2020.228449228449.
[58] C. Chao, C. Hsieh, W. Ke, L. Lee, Y. Lin, H. Liu, S. Gu, C. Fu, R. Juang, B.C. Mallick, Y.A. Gandomi, C. Su, Roll-to-roll atomic layer deposition of titania coating on polymeric separators for lithium ion batteries, J. Power Sources 482 (2021), 228896, https://doi.org/10.1016/j.jpowsour.2020.228896228896.
[59] Y. Xu, L. Gao, L. Shen, Q. Liu, Y. Zhu, Q. Liu, L. Li, X. Kong, Y. Lu, H.B. Wu, Ion-transport-rectifying layer enables li-metal batteries with high energy density, Matter 3 (2020) 1685–1700, https://doi.org/10.1016/j.matt.2020.08.0111685.
[60] B. Qiao, G.M. Leverick, W. Zhao, A.H. Flood, J.A. Johnson, Y. Shao-Horn, Supramolecular regulation of anions enhances conductivity and transference number of lithium in liquid electrolytes, J. Am. Chem. Soc. 140 (2018) 10932–10936, https://doi.org/10.1021/jacs.8b0591510932.
[61] B. Kumar, From colloidal to composite electrolytes: properties, peculiarities, and possibilities, J. Power Sources 135 (2004) 215–231, https://doi.org/10.1016/j.jpowsour.2004.04.038215.
[62] P. Zhang, L.C. Yang, L.L. Li, M.L. Ding, Y.P. Wu, R. Holze, Enhanced electrochemical and mechanical properties of P(VDF-HFP)-based composite polymer electrolytes with SiO_2 nanowires, J. Membr. Sci. 379 (2011) 80–85, https://doi.org/10.1016/j.memsci.2011.05.04380.
[63] S. Takeda, Y. Saito, H. Yoshitake, Restricted diffusion of lithium ions in lithium secondary batteries, J. Phys. Chem. C 124 (2020) 25712–25720, https://doi.org/10.1021/acs.jpcc.0c0769325712.
[64] S. Sheng, L. Sheng, L. Wang, N. Piao, X. He, Thickness variation of lithium metal anode with cycling, J. Power Sources 476 (2020), 228749, https://doi.org/10.1016/j.jpowsour.2020.228749228749.
[65] B. Bitzer, A. Gruhle, A new method for detecting lithium plating by measuring the cell thickness, J. Power Sources 262 (2014) 297–302, https://doi.org/10.1016/j.jpowsour.2014.03.142.
[66] L. Sheng, Y. Wu, J. Tian, L. Wang, J. Wang, Y. Tang, H. Xu, X. He, Impact of Lithium-Ion Coordination on Lithium Electrodeposition, ENERGY & ENVIRONMENTAL MATERIALS, 2021, https://doi.org/10.1002/eem2.12266.